A toy example of electrical impedance imaging using computational inference

Erfang Ma and Colin Fox
*Department of Physics, University of Otago, Box 56, Dunedin, NEW ZEALAND.
Email: ma@physics.otago.ac.nz

Abstract: We present an example of reconstruction in a toy example of electrical impedance tomography. Reconstructed images are computed using Bayesian inference by Markov chain Monte Carlo (MCMC) sampling implemented using a single-site Metropolis-Hasting algorithm.

Keywords: Inverse problem, Bayesian inference, EIT, MCMC

1 Introduction

Figure 1 shows a phantom conductivity that we use to generate a toy example of imaging. The imaging problem is to recover the spatially varying electrical conductivity from boundary measurements of current and voltage, often called electrical impedance tomography (EIT). The phantom occupies a square region, and has pixel-wise constant values of 4 (black) and 3 (white) in arbitrary units of conductivity. Measurements are made at 16 point electrodes (i.e. of no width) on the boundary (see Figure 2). This is same setup as used in [8].

In EIT, we normally inject a set of currents $\left\{\boldsymbol{j}_E^i, i=1,2,\ldots,k\right\}$ in different pattern through these electrodes and measure the resulting potentials at electrodes $\left\{\boldsymbol{u}_E^i, i=1,2,\ldots,k\right\}$. The set of measurements is the current-voltage pairs $\left\{\left(\boldsymbol{j}_E^i, \boldsymbol{u}_E^i\right), i=1,2,\ldots,k\right\}$. The imaging problem is to estimate the conductivities from these measurements [5].

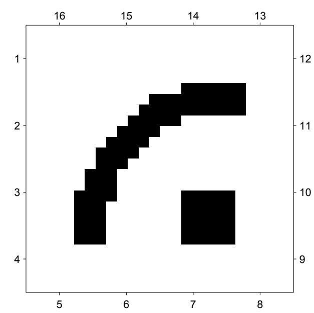

Figure 1: The phantom conductivity used in the toy example of EIT

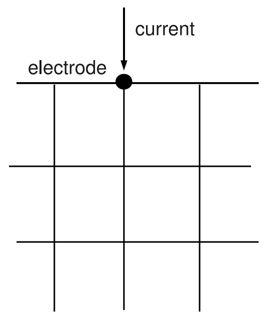

Figure 2: Diagram showing a point electrode

2 MCMC

In the Bayesian approach to EIT, the conductivity $\boldsymbol{\sigma}$ is treated as a random variable. The *posterior probability distribution* over $\boldsymbol{\sigma}$, given measurements of current and potential $f\left(\boldsymbol{\sigma} \mid \boldsymbol{u}_E, \boldsymbol{j}_E\right)$, is the focus of subsequent inference [5] [3].

Here, we employ a single-component Metropolis-Hastings algorithm [7] [9] to explore the posterior distribution and to obtain a set of samples $\boldsymbol{\sigma}^1, \boldsymbol{\sigma}^2, \ldots, \boldsymbol{\sigma}^n$ from this multivariate distribution. The algorithm is comprised of iterations $\boldsymbol{\sigma}^k = \left(\sigma_1^{(k)}, \sigma_2^{(k)}, \ldots, \sigma_m^{(k)}\right) \longrightarrow \boldsymbol{\sigma}^{k+1}$ each of which involves the following three steps

1 $\boldsymbol{\sigma}^k \rightarrow \boldsymbol{\sigma}' = \left(\sigma_1^{(k)}, \sigma_2^{(k)}, \ldots, \sigma_{i-1}^{(k)}, \sigma_i', \sigma_{i+1}^{(k)}, \ldots, \sigma_m^{(k)}\right)$.
Here $\sigma_i' = \sigma_i^k + z_i$, with $z_i \sim N(0, \sigma_{z_i})$

2 compute acceptance probability $a(\boldsymbol{\sigma},\boldsymbol{\sigma}') = \dfrac{f(\boldsymbol{\sigma}' \mid \boldsymbol{u}_E, j_E)}{f(\boldsymbol{\sigma} \mid \boldsymbol{u}_E, j_E)}$

3 accept update $\boldsymbol{\sigma}^{(k+1)} = \boldsymbol{\sigma}'$ with probability $\min\{1, a(\boldsymbol{\sigma},\boldsymbol{\sigma}')\}$.

Note that the normalization constant in the posterior distribution is not needed for the computation of acceptance probability, since

$$f(\boldsymbol{\sigma} \mid \boldsymbol{u}_E, \boldsymbol{j}_E) = \frac{f(\boldsymbol{u}_E \mid \boldsymbol{\sigma}, \boldsymbol{j}_E)\cdot f(\boldsymbol{\sigma})}{\int f(\boldsymbol{u}_E \mid \boldsymbol{\sigma}, \boldsymbol{j}_E)\cdot f(\boldsymbol{\sigma})\mathrm{d}\sigma}$$

hence,

$$a(\boldsymbol{\sigma},\boldsymbol{\sigma}') = \frac{f(\boldsymbol{u}_E \mid \boldsymbol{\sigma}', \boldsymbol{j}_E)\cdot f(\boldsymbol{\sigma}')}{f(\boldsymbol{u}_E \mid \boldsymbol{\sigma}, \boldsymbol{j}_E)\cdot f(\boldsymbol{\sigma})} \tag{1}$$

The prior distribution $f(\boldsymbol{\sigma})$ here [6] is

$$f(\boldsymbol{\sigma}) \propto \exp\left\{\beta \sum_{i\sim j} s(\sigma_i - \sigma_j)\right\}, \qquad \boldsymbol{\sigma} \in [2.5, 4.5]^m \tag{2}$$

where $s(.)$ is the tricube function [2]

$$s(d) = \begin{cases} \frac{1}{d_0}\left(1 - |d/d_0|^3\right)^3 & \text{if} - d_0 < d < d_0 \\ 0 & \text{if} |d| \geq d_0 \end{cases}.$$

The notation $i \sim j$ in the summation in equation 2 indicates an edge in the graph of Markov random field, as depicted in Figure 3. Figure 4 shows a realization from this prior distribution. We can see that this model allows abrupt changes of intensity in the image, which is a important feature for this application.

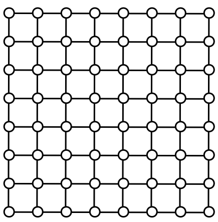

Figure 3: Graph of first order Markov random field corresponding to the pixel lattice

Evaluating the likelihood term $f(\boldsymbol{u}_E \mid \boldsymbol{\sigma}', j_E)$ involves solving a boundary value problem (BVP) in order to compute the forward map.

3 Forward Map

If noise in the forward map is modeled as

$$\boldsymbol{u}_E = \boldsymbol{u}_E^0(\boldsymbol{\sigma}, \boldsymbol{j}_E) + \boldsymbol{n} \tag{3}$$

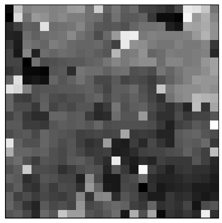

Figure 4: A realization from the prior showing typical properties

where $\boldsymbol{n} \sim N(0, \sigma_n \boldsymbol{I})$, then the likelihood function is

$$f(\boldsymbol{u}_E \mid \boldsymbol{\sigma}, \boldsymbol{j}_E) = \exp\left\{-\frac{1}{2\sigma_n^2}\|\boldsymbol{u}_E - \boldsymbol{u}_E^0(\boldsymbol{\sigma}, \boldsymbol{j}_E)\|_2^2\right\} \tag{4}$$

up to a constant of proportionality that does not depend on $\boldsymbol{\sigma}$. Here $\boldsymbol{u}_E^0(\boldsymbol{\sigma}, \boldsymbol{j}_E)$ is potential at electrode $u|_E$, in which the potential u is the solution of the BVP

$$\begin{aligned} -\nabla\cdot\sigma\nabla u &= 0 \qquad \Omega \\ -\sigma\frac{\partial u}{\partial n} &= j_E \qquad \partial\Omega \end{aligned}$$

We use the finite element method (FEM) to solve this BVP. The weak form of the BVP is

$$\int_\Omega (\nabla\cdot\sigma\nabla u)\cdot v = 0 \tag{5}$$

where v is the test function. Applying Green's identity we have

$$\int_\Omega \boldsymbol{\sigma}\nabla u\cdot\nabla v = \int_{\partial\Omega}\boldsymbol{\sigma}\frac{\partial u}{\partial n}\cdot v. \tag{6}$$

The associated quadratic form gives the forms for the components in the stiffness matrix $\boldsymbol{K}$ and load vector $\boldsymbol{f}$ in the FEM system

$$\boldsymbol{K}\boldsymbol{u} = \boldsymbol{f}. \tag{7}$$

They are

$$K_{ij} = \int_\Omega \sigma\nabla\phi_i\nabla\phi_j = \sum_{e=1}^{E}\int_{\Omega_e}\sigma\nabla\psi_i\nabla\psi_j$$

and

$$f_i = \int_{\partial\Omega}\sigma\frac{\partial u}{\partial n}\phi_i = \sum_b\int_{\Gamma_b}\sigma\frac{\partial u}{\partial n}\psi_i.$$

We use bilinear elements to interpolate within each (square) pixel. The 4×4 local stiff matrix is

$$\left[\int_{\Omega_e}\nabla\psi_i\psi_j\right] = \frac{1}{6}\begin{pmatrix} 4 & -1 & -2 & -1 \\ -1 & 4 & -1 & -2 \\ -2 & -1 & 4 & -2 \\ -1 & -2 & -1 & 4 \end{pmatrix}.$$

The force vector $\boldsymbol{f}$ depends on the current pattern injected. In this paper, we inject a current at one of the 16 electrodes and extract the current uniformly around the boundary. This procedure is repeated 16 times with each electrode taking turn as being an injector. So there is 16 sets of measurements overall, so we assemble the force vectors into the matrix $\boldsymbol{F}$ having 16 columns, with each column corresponding to a set of measurements. If I amount of current is injected and there are m number of nodes on the boundary, the nonzero element of the ith column of $\boldsymbol{F}$, are at the entry of boundary nodes, and of value $1/m$, except for the entry of injector being $\frac{m-1}{m}$.

The steps required for a computation of the acceptance ratio $a\left(\boldsymbol{\sigma}, \boldsymbol{\sigma}'\right)$ are illustrated in the diagram in Figure 5.

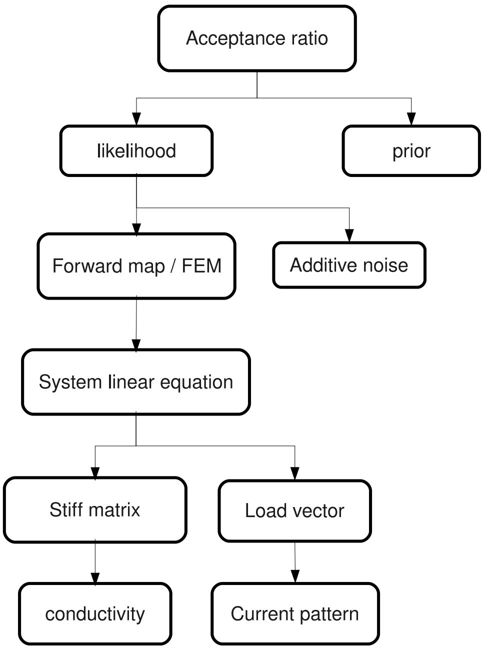

Figure 5: Diagram of computational steps for the acceptance ratio

4 Numerical Results

We started the chain at $\boldsymbol{\sigma}_0 = (3, 3, \ldots, 3)$, and didn't stop until $80,000 \times m$ simulations had been completed. During the time, we recorded the state of $\boldsymbol{\sigma}$ every 10 scans ($10 \times m$ iterations).

We also adjusted the step size σ_{z_i} in the proposal step to make sure that the acceptance rate for each pixel is within $[30\%, 70\%]$. Specifically, σ_{z_i} for the pixels near electrodes are set to be relatively small and get larger for the pixels towards the centre. The exception is those pixels at the four corners, which have the biggest step size. An image of step size is show in Figure 6.

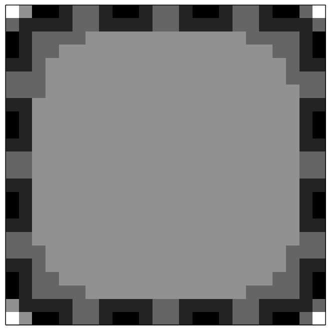

Figure 6: Image of step size as a function of pixel. Brightness is proportional to σ_{z_i}

It is easy for us to provide a rough estimate of burn-in from the trace plot of log-prior (Figure 7) and that of log-likelihood (Figure 8), which is about first $40,000$ samples.

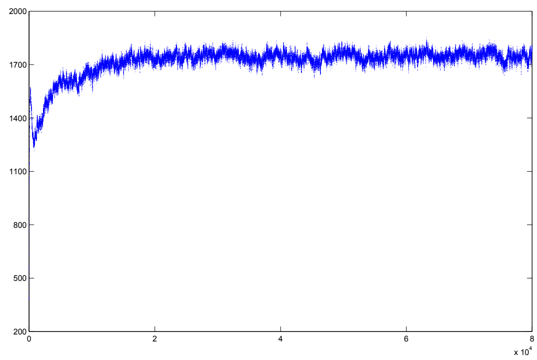

Figure 7: Trace of log-prior

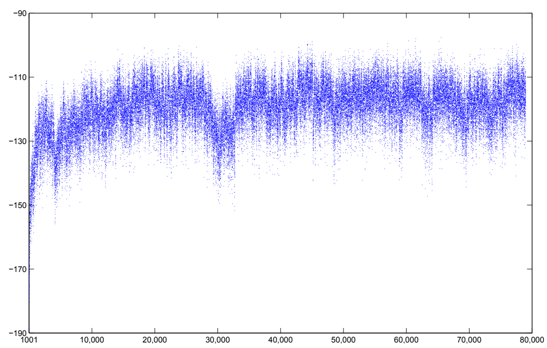

Figure 8: Trace of log-likelihood

Four realizations after the burn-in, which are separated by $1,000$ scans ($1,000 \times m$ iterations), are shown in Figure 9.

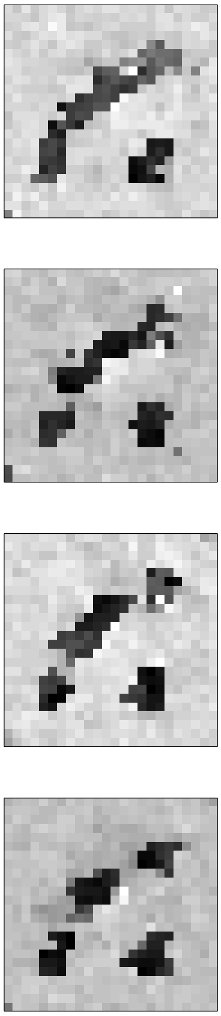

Figure 9: Four samples from the posterior distribution

Traces of the conductivity at three pixels in the image are shown in Figure 10. The location of the three pixels are depicted as red, blue, and green circles in Figure 14. We see that the sampler moves closely around desired low conductivity during the course, while it is jumping up and down from time to time in the dimension of the other two pixels. This is in accordance with the marginal distributions for these pixels (Figure 11 12 13). The marginal distribution for pixel red has only one mode, while the other two marginal distributions are bimodal.

All these results show that single-site Metropolis-Hasting algorithm did not do a bad job in sampling this high-dimensional distribution.

If any single estimator of conductivity is of interest, posterior mean (Figure 14) and marginal posterior mode (Figure 15)are two popular choices [4]. As we see in Figure 14, most of the uncertainty is about boundary of high conductivity region. The discrepancy between marginal posterior mode (Figure 15) and original one (Figure 1) happens to be around the same place.

However, note that $80,000$ iterations had been done to achieve the above result, and it took quite a few days to run

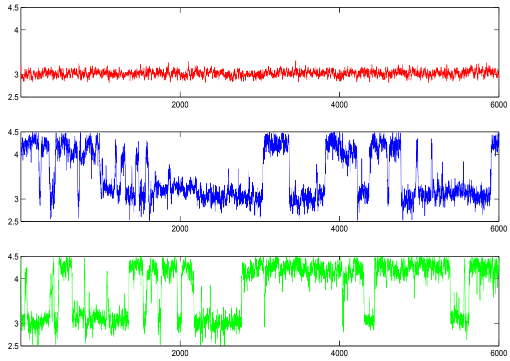

Figure 10: traces of three pixels during the MCMC run

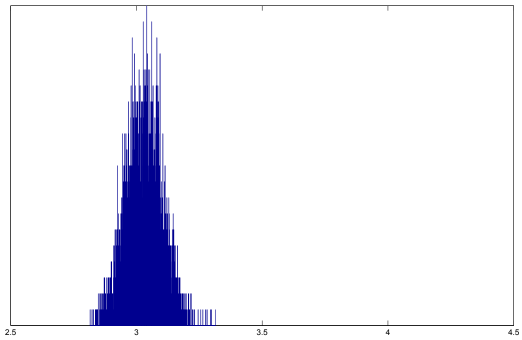

Figure 11: Sample marginal distribution for pixel red

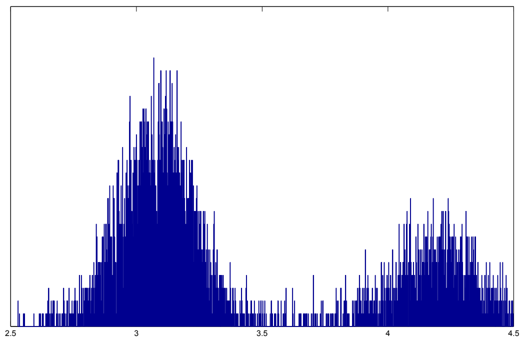

Figure 12: Sample marginal distribution for pixel blue

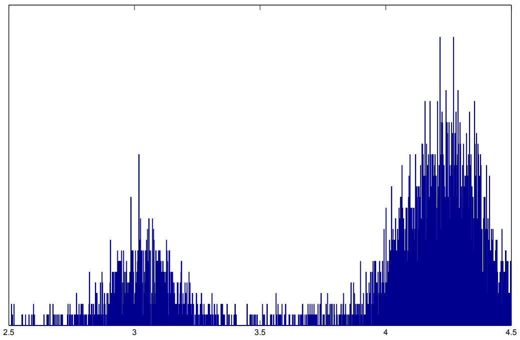

Figure 13: Sample marginal distribution for pixel green

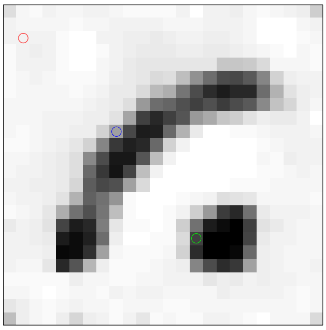

Figure 14: Posterior mean conductivity

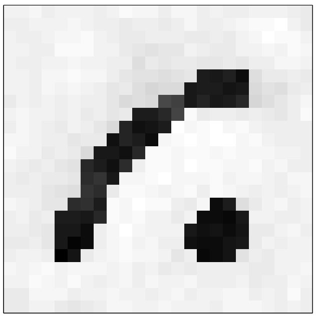

Figure 15: Marginal posterior mode

this long simulation in Matlab. We also mention that about 99% of CPU time had been spent on solving the system of linear equation in FEM stage for the forward map.

5 Conclusion and further work

Single-site Metropolis-Hasting algorithm can be used to sample the posterior distribution arising in Bayesian inference in EIT, as long as speed is not a top priority. Future work could focus on alternative MCMC algorithms which are more efficient and fast in this appplication, e.g. delayed acceptance MCMC [1].

References

[1] J.A. Christen and C.Fox, *MCMC using an approximation* J.Comput. Graph. Stat. 14 (2005), pp. 795-810.

[2] W.S. Cleveland *Robust Locally Weighted Regression and Smoothing Scatterplots* Journal of the American Statistical Association, 74 (1979), 829-836.

[3] C. Fox *Recent advances in inferential solutions to inverse problems* Inverse Problems in Science and Engineering Vol. 16, No. 6, September 2008, 797-810.

[4] C. Fox and G. Nicholls *Exact map states and expectations from perfect sampling: Greig, Porteous and Seheult revisited,* in *Twentieth International Workshop on Bayesian Inference and Maximum Entropy Methods in Science and Engineering*, A.M. Djafari, ed., AIP, Melville, New York, USA, 2000, pp. 252-263.

[5] C. Fox and G. Nicholls *Sampling Conductivity images via MCMC* The art and science of Bayesian image analysis. Proceedings of the Fifth Valencia Interntional Meeting, June 5-9, 1997

[6] S. Geman. and D. McClure *Statistical methods for tomographic image reconstruction* Bulliten of the International Statistical Institute, 52, no.4 (1987) 5-21.

[7] N. Metropolis, M. Rosenbluth, A. Teller, and E. Teller "Equations of state calculations by fast computing machines" *Journal of Chemical Physics*, 21, (1953) 1087-1091.

[8] J. D. Moulton, C. Fox, and D. Svyatskiy *Multilevel Approximations in Sample-Based Inversion from the Dirchlet-to-Neuman Map.* Tech. Rep. LA-UR 07-7958, Mathematical Modeling and Analysis Group, Los Alamos National Laboratory.(2007)

[9] A. F. M. Smith, G. O. Roberts *Bayesian Computation via the Gibbs Sampler and Related Markov Chain Monte Carlo Method* J. R. Statist. Soc. B 55, No.1 (1993) pp. 3-23